Supporting Information for "Integrated Effects of Site Hydrology and Vegetation on Exchange Fluxes and Nutrient Cycling at a Coastal Terrestrial-Aquatic Interface"

Bing Li[1], Zhi Li[1], Jianqiu Zheng [1], Peishi Jiang [1], James Holmquist [3], Peter J. Regier [1], G.E. Hammond [1], Nicholas D. Ward [1], Allison Myers-Pigg[1], Roy Rich[3], Wei Huang [2], Theresa A. O'Meara [2], Stephanie C. Pennington [1], Patrick Megonigal [3], Vanessa L Bailey [1], Xingyuan Chen [1]

[1]Pacific Northwest National Laboratory, Richland, WA, USA 99352.
[2]Oak Ridge National Laboratory, Oak Ridge, TN, USA 37830.
[3]Smithsonian Environmental Research Center, Edgewater, MD, USA 21037.

Contents

Introduction

The supporting information consists of five sections of text. Text S1 provides information about the generation of two dimensional (2-D) model and mesh. Text S2 explains the governing equations utilized in ATS. Text S3 presents hydro-geological data and parameters used in the model. Text S4 includes ecological data relevant to vegetation-related processes. Lastly, Text S5 illustrates the setup of simulations and part of results.

Corresponding author: Xingyuan, Chen, `Xingyuan.Chen@pnnl.gov`

Text S1: Developing Two Dimensional Model and Mesh.

A 2-D transect was chosen at the TEMPEST site, spanning from GW2 to GW8. The selection of this transect was based on both the field sampling locations and the completeness of the data, and it was subsequently extended towards the ocean. By utilizing this transect, we enable the modeling of various land covers such as wetlands, marshes, and open water. For all cases considered in this paper, the meshes were generated using watershed workflow [*Coon and Shuai*, 2022]. Initially, we utilized the digital elevation model Lidar data for the entire state of Maryland, which can be obtained from the following URL: [https://imap.maryland.gov/Pages/lidar-dem-download-files.aspx]. This data allowed us to accurately capture the elevation and topography of the domain at a resolution of 0.3m/1ft. Then, mesh sensitivity analysis has been performed with progressively refined meshes for both surface and subsurface domain. The most refined meshes had an average grid size of about 0.05 m near the surface-subsurface interface.

Text. S2. The Governing Equation used in ATS.

Here, the diffusive wave model [*Lal*, 1998] of overland flow and Richards's [*Richards*, 1931] model for variably saturated flow have been used to govern the fluid motion in the river and the sediment groundwater, respectively.

$$\frac{\partial}{\partial t}(n_l h) + \nabla \cdot \mathbf{q_s} = Q \tag{1}$$

$$\mathbf{q_s} = -n_l h \frac{h^{4/3}}{n_{mann}\sqrt{|\nabla Z_s + \epsilon|}} \nabla(h + Z_s) \tag{2}$$

where h is surface water depth $[m]$, Q is source $[mol\ m^{-2}\ s^{-1}]$ term, it includes the source/sink terms (rain, snow melt, and evaporation) and exchanged water from the subsurface [*Coon et al.*, 2020], n_{mann} is Manning coefficient $[s\ m^{-1/3}]$, Z_s is surface elevation $[m^{-1}]$, ϵ is regularization $[m]$, $\mathbf{q_s}$ is the flux of surface water $[mol\ m^{-1}\ s^{-1}]$.

$$\frac{\partial}{\partial t}(\phi n_l s) + \nabla \cdot \mathbf{q} = Q_g \tag{3}$$

$$\mathbf{q} = -n_l \frac{k_r k}{\mu}(\nabla p + \rho \mathbf{g}) \tag{4}$$

where ϕ is soil porosity [-], n_l is molar water density $[mol\ m^{-3}]$, k_r is relative permeability [-], k is absolute permeability $[m^2]$, μ is dynamic viscosity $[Pa\ s]$, ρ is the mass water density $[kg\ m^{-3}]$, $\mathbf{g}$ is the gravity $[m\ s^{-2}]$.

The reactive transport of solute is modeled with an advection-diffusion/dispersion equation in both surface and subsurface domain.

$$\frac{\partial \Theta_s X_1}{\partial t} - \nabla \cdot (\mathbf{h D_s} \nabla \eta \mathbf{X_1}) + \nabla \cdot \mathbf{q_s X_1} = Q X_1 + R_s \tag{5}$$

$$\frac{\partial \Theta_s X_2}{\partial t} - \nabla \cdot (\phi \mathbf{S_w D_g} \nabla \eta \mathbf{X_2}) + \nabla \cdot \mathbf{q_s X_2} = Q X_2 + R_g \tag{6}$$

where X_1 and X_2 are the solute concentration of surface and subsurface water (mol fraction), D_s is the hydrodynamic dispersion coefficient in surface domain , X is the concentration in the source term, R_s is the concentration of the kinetic reactions in the surface domain, D_g is the hydrodynamic dispersion coefficient in subsurface domain, R_g is the concentration of the kinetic reactions in the subsurface domain.

The surface water balance in terms of sources and sinks is expressed as follows:

$$Q_s = SM + D_{rain} + Th_{rain} - E \tag{7}$$

Here, SM represents snowmelt, D_{rain} represents the drainage of liquid water from the canopy, Th_{rain} represents the throughfall of rain, and E represents evaporation from bare soil. These terms are all measured in units of meters per second $[m/s]$.

In addition to the surface water balance, water conservation is also considered in the snowpack and canopy. The conservation equations for water in the snowpack and canopy account for the accumulation and loss of water within these compartments.

$$\frac{d\Theta_{snow}}{dt} = D_{snow} + Th_{snow} - SM \tag{8}$$

$$\frac{d\Theta_{canopy}}{dt} = I - D_{snow} - D_{rain} - E_{canopy} \tag{9}$$

Interception and throughfall are partitioned based on leaf area, and drainage or dripping from the canopy to the land surface is given by a simple exponential decay in which canopy storage decays back to a target maximum storage which is also a function of leaf area.

$$I = \beta(1 - e^{-0.5LAI}(P_{rain} + P_{snow}) \tag{10}$$

$$Th_i = [1 - \beta((1 - e^{-0.5LAI})]P_i, i = (rain, snow) \tag{11}$$

$$D_i = max(0, \frac{P_i}{P_{rain} + P_{snow}} \frac{\Theta_{canopy} - \Theta_{sat}}{\tau}) \tag{12}$$

$$\Theta_{sat} = \theta_{sat} LAI \tag{13}$$

Text S3: Hydrogeological Data and Parameters used in Integrated Models.

Information on geologic formations, depth to bedrock, soil texture, and soil properties have been obtained from various sources, including NLCD (`https://www.usgs.gov/centers/eros/science/national-land-cover-database`), GLYHMPS, SoilGrids 2017 [*Hengl et al.*, 2017], and SSURGO (`URL:https://www.nrcs.usda.gov/resources/data-and-reports/soil-survey-geographic-database-ssurgo`). We obtain soil information from the soil database using the watershed workflow [*Coon and Shuai*, 2022]. Highly permeable soils and low permeable soils have been assigned spatially. Therefore, we set different soil porosity, soil hydraulic conductivity, and van Genuchten water retention parameters for the two layers (see parameter values in Table S1 and Table S2.)

Table S1. Constant values of model parameters.

Parameter	Value	Parameter	Value
hydrostatic water density (kg m^{-3})	1000	Gravity (m/s^2)	9.80665
Sea level standard atmospheric pressure (pa)	101325	Manning coefficient (-)	0.1825
Molar density (kg/m^3)	997	Water dynamic viscosity (Pa · s)	0.00089

Table S2. Hydrogeological Properties by Region

Region	Permeability Value	Base Porosity Value	van Genuchten n [-]	van Genuchten alpha [Pa^{-1}]	Residual Saturation [-]
GLHYMPS-922332	1e-13	0.22	2.0	0.000294	0.01
GLHYMPS-922379	1.2589254e-11	0.28	2.0	0.002923	0.01
NRCS-137738	1.1644531e-12	0.45394173	1.4457	0.000158	0.1957
NRCS-137805	1.5037828e-12	0.67756012	1.4586	0.000035	0.188253
NRCS-609565	5.0131429e-13	0.3913441	1.483322	0.000181	0.1951
bedrock	1e-16	0.15	3.0	0.000011	0.01

Text S4: Ecological Data and Parameters used in Integrated Model.

Additionally, land cover types and meteorology data and plant types have been collected using MODIS and Daymet data sources. For example, precipitation, evaporation, and transpiration have been considered as the source or sink term for the domain shown in above equations.

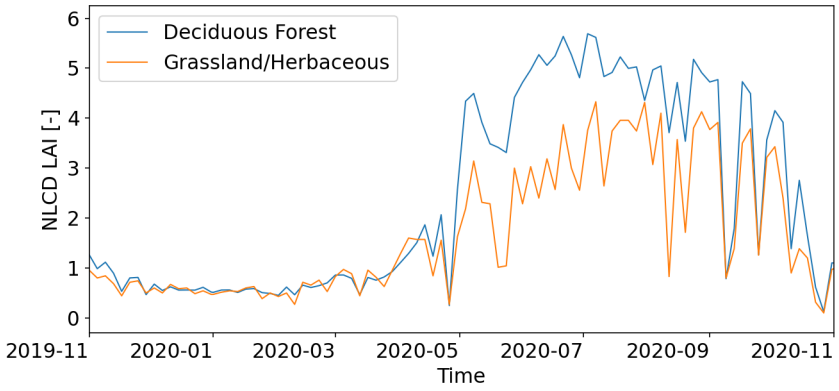

Figure S1. The leaf area index for two main vegetation types.

This study utilized default values for certain land cover parameters, such as the rooting depth curve and canopy albedo, which were sourced from the CLM technical note paper [*Oleson et al.*, 2013].

Text S5: Setup of the simulation and results

To have a properly initialized condition and accurately simulate the system, hot spin-up, and cold spin-up are used for both flow and reactive parts. Using the steady-state conditions, constant tide elevation and upland water level, we run the cold spin-up for 1000 years to ensure that the model is properly initialized with the water level. The process involves a 10-year hot spin-up using both dynamic flow boundary conditions and constant boundary conditions for species. This process helps to ensure that the model has a dynamic equilibrium condition. To be specific, the tidal dynamics as boundary condition at the right face domain. The precipitation is from Daymet data, dynamic tidal is from USGS tidal gage 01492600. The time step size in all simulations was allowed to be dynamically adjusted to satisfy a specified maximum Courant number of 0.1. The simulations were run on the COMPASS supercomputer (`URL:https://compass.pnnl.gov`) using 16 cores in parallel. The hot spin-up boundary condition is presented in Figure S9.

Figure S4 and Figure S5 showcase the temporal evolution of exchange fluxes for scenario 2 and scenario 3 over a specific time period. The spatial distribution of fluxes highlights areas of intense interaction and exchange between the surface and subsurface domains. As we expected, dynamic tide influence transition, wetland, and open water regions. High tide induced flooding process will enhance the downwelling flux at the transition region. Meanwhile, the downwelling flux located at the upland region is dominated by the precipitation only. The strongest downwelling flux had been seen during the heavy rain event (day 218). The figure provides valuable insights into the complex hydrody-

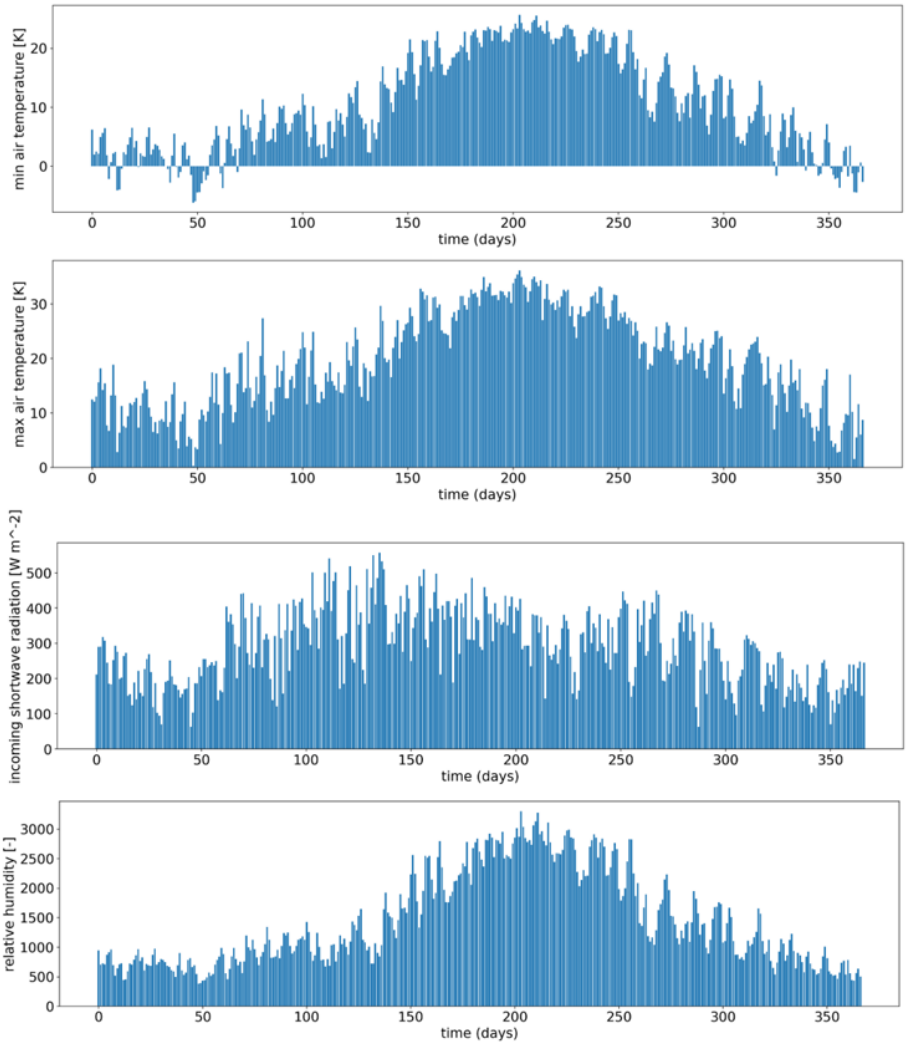

Figure S2. Relative humidity, temperature, and incoming shortwave radiation.

Table S3. Parameter List for Deciduous Forest and Grassland

Parameter	**Deciduous Forest**	**Grassland**
Rooting depth max [m]	10	4
Rooting profile alpha [-]	6	11
Rooting profile beta [-]	2	2
Mafic potential at fully closed stomata [Pa]	224000	275000
Mafic potential at fully open stomata [Pa]	3500	7400
Leaf on time [doy]	-1	-1
Leaf off time [doy]	-1	-1
Priestley-Taylor alpha of snow [-]	1.26	1.26
Priestley-Taylor alpha of bare ground [-]	1.26	1.26
Priestley-Taylor alpha of canopy [-]	1.26	1.26
Priestley-Taylor alpha of transpiration [-]	0.63	0.63
Albedo of bare ground [-]	0.4	0.4
Emissivity of bare ground [-]	0.98	0.98
Albedo of canopy [-]	0.1	0.11
Emissivity of canopy [-]	0.95	0.95
Beer's law extinction coefficient, shortwave [-]	0.6	0.6
Beer's law extinction coefficient, longwave [-]	5	5
Snow transition depth [m]	0.02	0.02
Dessicated zone thickness [m]	0.1	0.1
Clapp and Hornberger b [-]	1	1

namic processes driven by tidal dynamics and varying precipitation, contributing to a better understanding of the flow dynamics within the studied system.

In our analysis, we examined the results and visualized the flow path and the distribution of tracers in Figure S6. Upon observing the flow path, we observed a fluid movement from right to left in the region extending from the left side to near the highest point on the left side. This directional flow is primarily influenced by the pressure gradient. Consequently, for this study, we utilized the water level height data from GW2 without investigating the impact of its dynamic changes on the results. Because, our numerical findings indicate that the variation in water level uphill had minimal effect on the TAI region within the chosen 2D model. Subfigure a shows the flow path within the 2-D transects at the end of spin-up run. The tracer distribution from rain and seawater, as depicted in subfigures B and C, reveals that the primary mixing region is situated within the transient and wetland areas. This observation highlights the significance of these regions in the overall mixing processes. To ensure a continuous transport of dissolved organic carbon (DOC) and nitrate by groundwater to the TAI region in our 2D model, we established the groundwater boundary by adding a constant concentration value to the leftmost side. We also introduced the same concentration value at the vertical location where the highest point is situated.

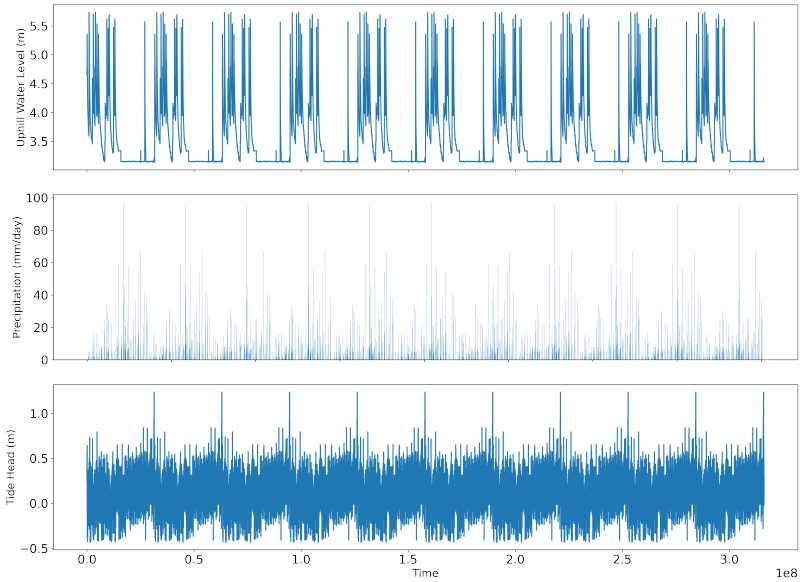

Figure S3. Uphill water level, precipitation, and tide head for hot spin up run.

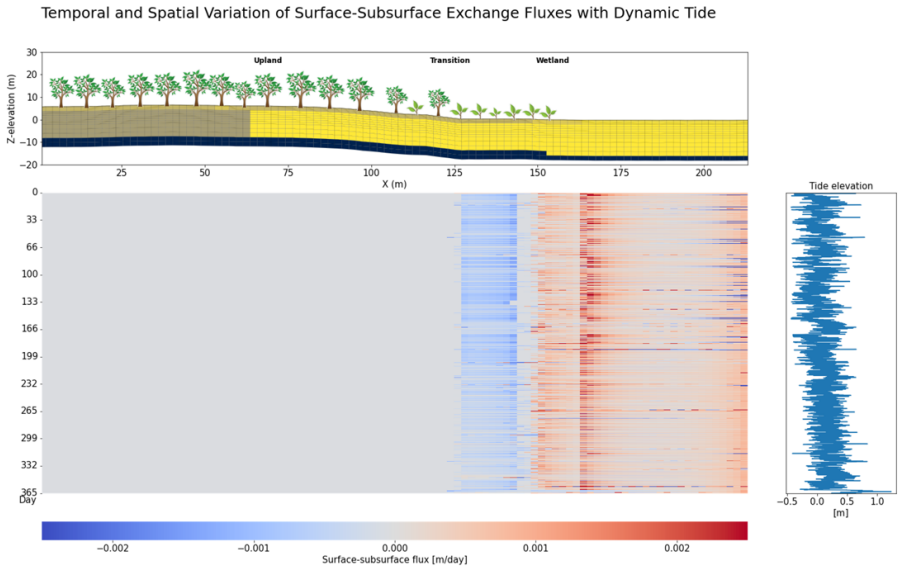

Figure S4. This figure shows the dynamic variations in flow exchange flux between the surface and subsurface domains, primarily influenced by tidal changes.

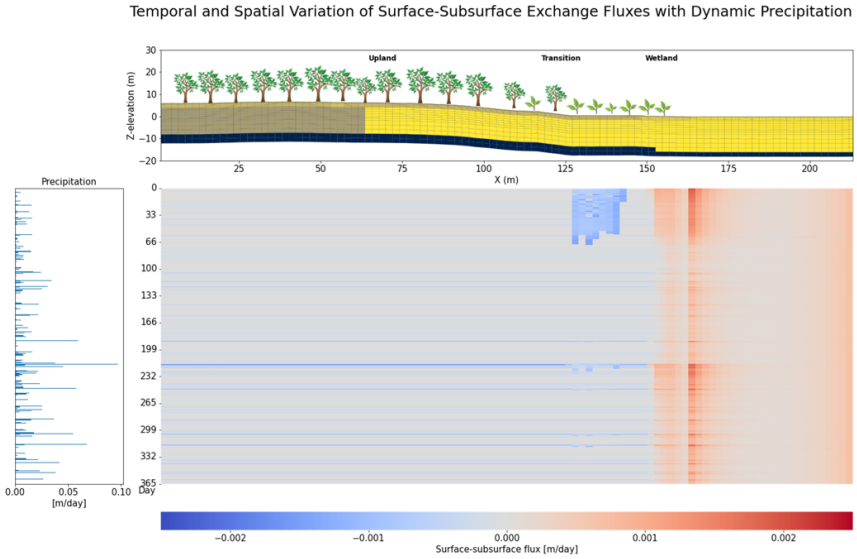

Figure S5. This figure exhibits the flow exchange flux between the surface and subsurface domains, which varies with dynamic precipitation.

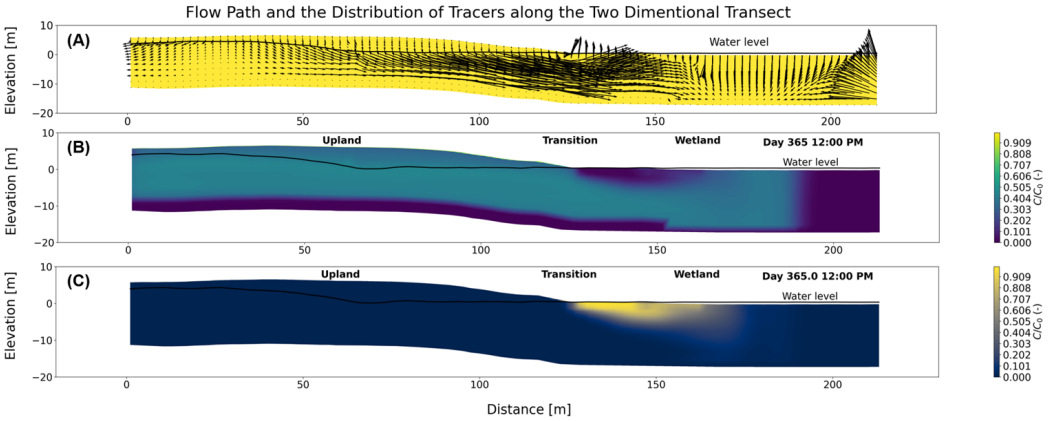

Figure S6. This figure illustrates the flow path and the distribution of tracers.

Dynamic exchange flux of DOC and nitrate had been analyzed for scenario one shown in Figure S7 and Figure S8. Strong upwelling fluxes of DOC and nitrate occurred in wetland and open water areas, mainly due to movement of groundwater. DOC and nitrate in surface domain carried by upwelling fluxes will in turn be transported to the transition zone with the seawater inundation process, and then we noticed downwelling fluxes of DOC and nitrate were formed within the transition zone. The intense of exchange fluxes affected by both precipitation and dynamic tide changes.

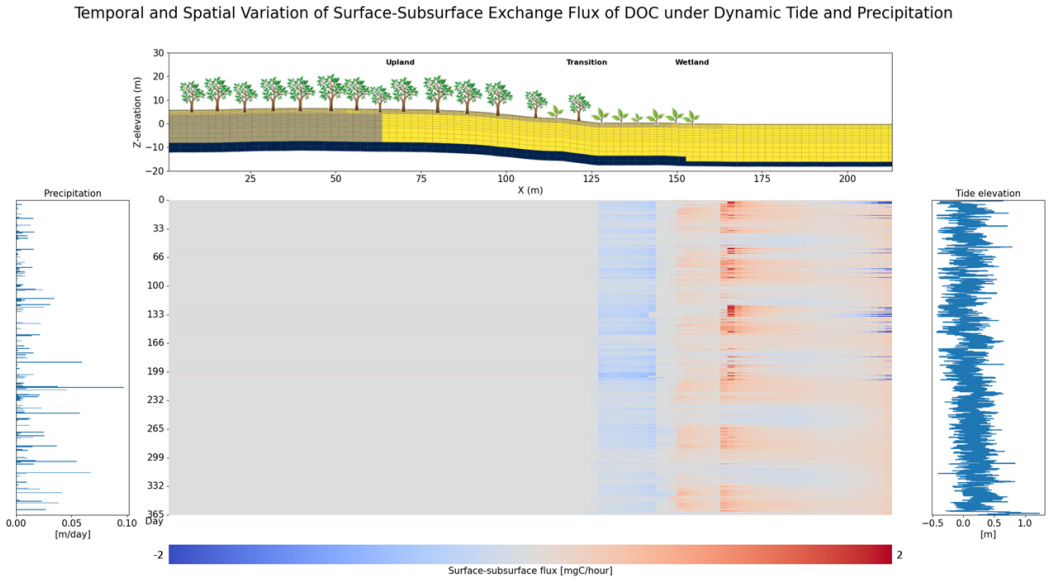

Figure S7. Heatmap of DOC exchange fluxes along a two-dimensional transect.

The dynamic of oxygen saturation had been shown below, from the spin-up simulation results. We found the hot zone is located in the transition and wetland regions in our case.

The comparison of exchange flux between Scenario 1 and Scenario 4 is illustrated in Figure S10. During the summer season, it was observed that the correlation between the two scenarios was low, indicating that the influence of canopy evapotranspiration on the exchange flow flux was more pronounced.

It is important to note that this approach illustrates the limitations of the 2D model, as in real-world scenarios, water level changes and material transport occur in directions perpendicular to the 2D model. The primary focus of this paper revolves around examining the hydrological and ecological process changes on chemical reactions within a 2D environment, hence the aforementioned setup was employed. Nevertheless, our results underscore the necessity of incorporating a 3D model for comprehensive analysis. In future perspectives, we outline our plan to conduct simulations using 3D models.

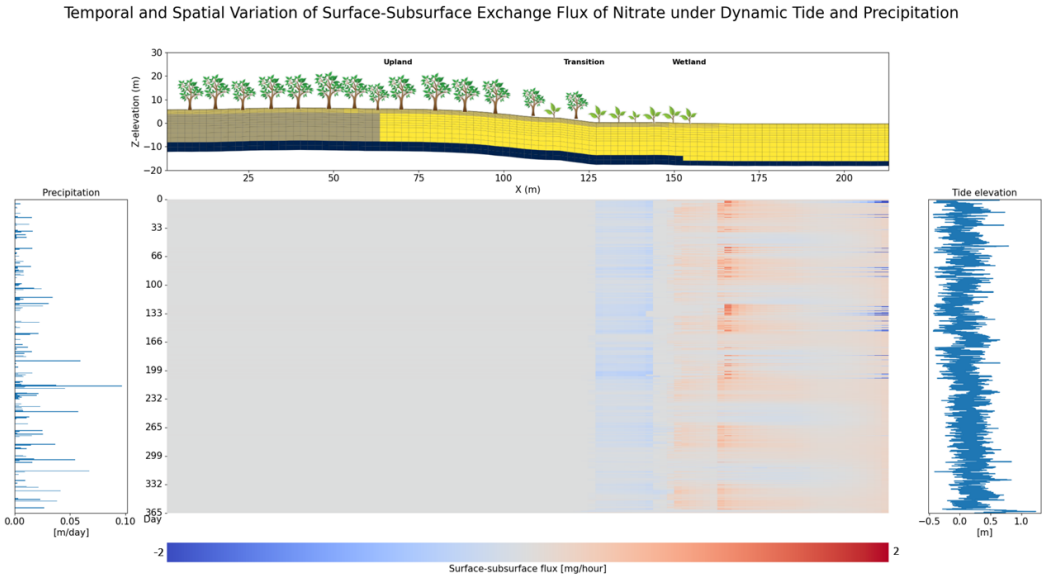

Figure S8. Heatmap of nitrate exchange fluxes along a two-dimensional transect.

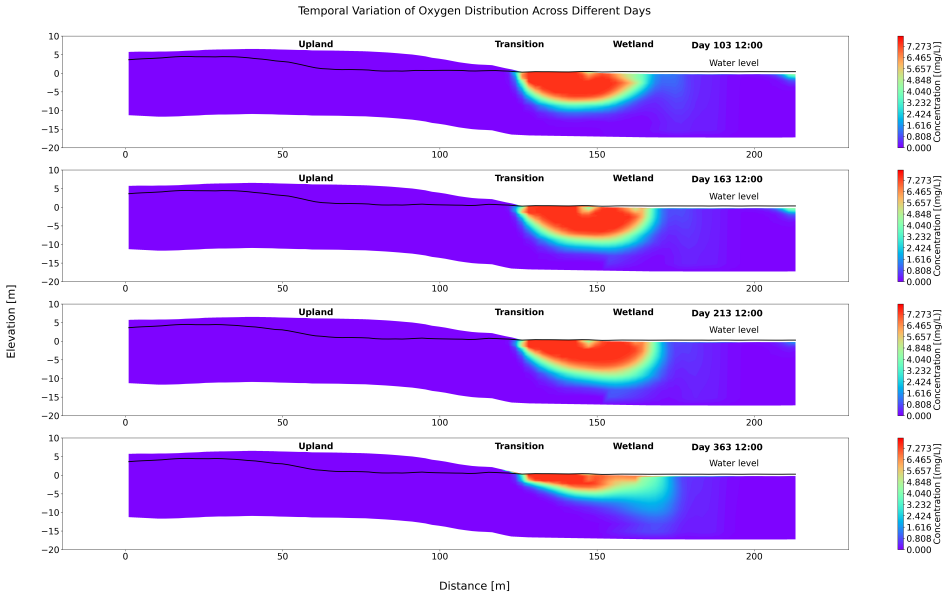

Figure S9. This figure illustrates the distribution of oxygen along the 2D transect, which varies with dynamic precipitation and tidal changes. Beneath the exchange flux area, the shape and size of the oxic zone change with time.

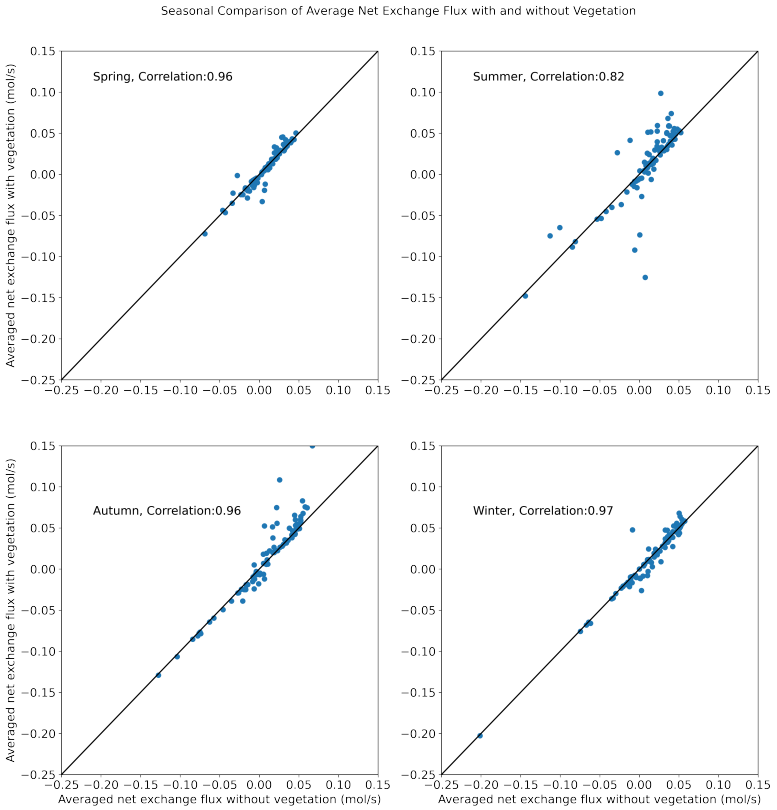

Figure S10. The plot shows the exchange flux comparison between cases with and without vegetation, during summer, the correlation is smallest among the four seasons.

References

Coon, E. T., and P. Shuai (2022), Watershed workflow: A toolset for parameterizing data-intensive, integrated hydrologic models, *Environmental Modelling & Software*, *157*, 105,502.

Coon, E. T., J. D. Moulton, E. Kikinzon, M. Berndt, G. Manzini, R. Garimella, K. Lipnikov, and S. L. Painter (2020), Coupling surface flow and subsurface flow in complex soil structures using mimetic finite differences, *Advances in Water Resources*, *144*, 103,701.

Hengl, T., J. Mendes de Jesus, G. B. Heuvelink, M. Ruiperez Gonzalez, M. Kilibarda, A. Blagotić, W. Shangguan, M. N. Wright, X. Geng, B. Bauer-Marschallinger, et al. (2017), Soilgrids250m: Global gridded soil information based on machine learning, *PLoS one*, *12*(2), e0169,748.

Lal, A. W. (1998), Weighted implicit finite-volume model for overland flow, *Journal of Hydraulic Engineering*, *124*(9), 941–950.

Oleson, K., D. Lawrence, G. Bonan, B. Drewniak, M. Huang, C. Koven, S. Levis, F. Li, W. Riley, Z. Subin, et al. (2013), Technical description of version 4.5 of the community land model (clm)(ncar technical note no. ncar/tn-503+ str). citeseer, *National Center for Atmospheric Research, PO Box*, *3000*, 555.

Richards, L. A. (1931), Capillary conduction of liquids through porous mediums, *Physics*, *1*(5), 318–333.